Crystal structure of urotropine under high pressure and non-hydrostatic stress-induced phase transitions in cage compounds

Piotr A. Guńka[*1], Anna Olejniczak[2], Samuele Fanetti[3,4], Roberto Bini[3,4,5], Ines E. Collings[†6], Volodymyr Svitlyk[6], Kamil F. Dziubek*[*3]*

[1]Faculty of Chemistry, Warsaw University of Technology, 00-664 Warszawa, Poland

[2]Faculty of Chemistry, Adam Mickiewicz University, 60-780 Poznań, Poland

[3]LENS, European Laboratory for Nonlinear Spectroscopy, 50019 Sesto Fiorentino, Italy

[4]Dipartimento di Chimica, Università degli Studi di Firenze, 50019 Sesto Fiorentino, Italy

[5]Instituto di Chimica dei Composti Organo-Metallici, CNR-ICCOM, 50019 Sesto Fiorentino, Italy

[6]European Synchrotron Radiation Facility, 38043 Grenoble, France

ABSTRACT

High-pressure behavior of hexamthyleneteramine (urotropine) was studied *in situ* using angle-dispersive single-crystal synchrotron X-ray diffraction (XRD) and Fourier transform infrared absorption (FTIR) spectroscopy. Experiments were conducted in various pressure transmitting media (helium and neon for XRD, nitrogen and KBr for FTIR experiments) to study the effect of deviatoric stress on phase transformations. Contrary to As_4O_6 arsenolite, a material of similar cage-like molecular structure, no pressure-induced helium penetration into the crystal structure was observed. Instead, two pressure-induced structural changes are observed. The first one is suggested by the following occurrences: (i) gradual quenching of the magnitudes of atomic displacement parameters, (ii) diminishing libration contribution to the experimental C−N bond length, (iii) discontinuity in calculated IR-active vibrational modes and (iv) asymptotically vanishing discrepancy between the experimental and DFT-calculated unit cell volume. All these features reach a plateau at ~4 GPa and can be attributed to a damping of molecular librations and atomic thermal motion, pointing to the existence of a second-order isostructural phase transition. The second transformation, with an onset at ~12.5 GPa is a first-order phase transition to a tetragonal structure, characterized by sluggish kinetics and considerable hysteresis upon decompression. However, it occurs only in non-hydrostatic conditions, induced by a deviatoric stress in the sample. This behavior finds analogies in similar cubic crystals built of highly symmetric cage-like molecules and may be considered a common feature of such systems. Last but not least, it is worth noting successful Hirshfeld atom refinements, carried out for the incomplete high-pressure diffraction data up to 14 GPa, yielded more realistic C−H bond lengths than the independent atom model.

INTRODUCTION

Hexamethylenetetramine (urotropine) is a heterocyclic organic amine with molecules of cage-like structure, composed of interconnected six-membered rings, each in the armchair conformation. Such a spatial atomic arrangement resembles that of carbon atoms in the diamond crystal structure and also many organic (like adamantane) and inorganic (like arsenolite form of arsenic trioxide, As_4O_6) molecules.[1,2] Urotropine was obtained for the first time in 1859 by Alexandr Butlerov, and has become an important precursor in synthetic industry in the production of phenolic, urea and formaldehyde resins or high energy density materials, such as hexogen and octogen.[3,4] Further applications include solid fuel tablets, vulcanization accelerators and anticorrosive agents.[5] While not found in terrestrial nature, urotropine is expected to be present in some comets, as it is an important component of refractory organic residues obtained by warming up photolyzed cometary ice analogues.[6] In crystal engineering, urotropine is known for being prone to form cocrystals (more than 500 structures present in the Cambridge Structural Database).[7] It can also act as a versatile ligand providing a basis for designing new coordination polymers, due to its capability of adopting various coordination modes.[8]

Noteworthy, urotropine was the first organic compound whose crystal structure was determined by X-ray diffraction. It was accomplished independently by two research groups, as early as in 1923.[9,10] Due to the high crystal symmetry and one independent molecule with the center of gravity at the origin of the unit cell, the number of symmetry-independent atoms and hence refined parameters is substantially reduced. This turned out to be critical for the final success of this undertaking, considering the crude methods and means available in the early days of structural analysis. Indeed, unlike the vast majority of organic compounds, urotropine crystallizes in a high symmetry space group $I\bar{4}3m$. In this respect, it is consistent with the

preference of other rigid cage-like organic molecules to pack in high symmetry space groups, *e.g.* solid adamantane (two ambient-pressure phases, $Fm\bar{3}m$ and $P\bar{4}2_1c$), cubane ($R\bar{3}$), dodecahedrane ($Fm\bar{3}$),[11] diamantane ($Pa\bar{3}$) [12] and also inorganic materials, *e.g.* As_4O_6 arsenolite ($Fd\bar{3}m$) [13] or isostructural Sb_4O_6 senarmontite[14], both made up from discrete adamantoid molecules. In all these structures, high-symmetry special positions coincide with the *center of gravity* of cage molecules. Any structural changes associated with crystal lattice symmetry lowering according to a group-subgroup relation, and in consequence site symmetry lowering, must be thus coupled to anisotropic distortion of the molecular environment and perturbation of the parent structure. Hence, behavior of solid molecular cage compounds in pressure-temperature space poses an especially intriguing subject to explore.

A prototypical member of this group, adamantane, a tricyclic saturated hydrocarbon, exists as a plastic crystal at ambient conditions (space group $Fm\bar{3}m$), which transforms to an ordered tetragonal phase ($P\bar{4}2_1c$) at temperature below 208.6 K or at high pressure above 0.5 GPa.[15] The ordered $R\bar{3}$ crystalline phase of cubane is a stable modification from 77 to 394 K [16] and also under high pressure up to 60 GPa[17]. The cubic $Fm\bar{3}$ form of dodecahedrane is stable up to 20 GPa according to Raman spectroscopy data.[18] High-pressure phase transformations of diamantane, a cage hydrocarbon that consists of two *face-fused* adamantane units, present *an especially interesting* case as they strongly depend on hydrostaticity of the environment.[19] Diamantane crystallizes in space group $Pa3$ at ambient conditions and while compressed in helium it shows no phase transitions up to 13 GPa, in silicone oil it transforms to a monoclinic phase with the onset of transition at 7 GPa, coinciding with the hydrostatic limit of the pressure-transmitting medium (PTM). Moreover, diamantane compressed without any PTM exhibits two phase transformations characterized by large hysteresis and sluggish transformation kinetics,

with the onsets at 0.15 GPa and 3.5 GPa. Both of these high-pressure structures could be indexed using monoclinic lattices.

Group 15 elements sesquioxides are other examples where behavior at high pressure is strongly influenced by nonhydrostatic conditions. With helium as the PTM, cubic $Fd\bar{3}m$ arsenolite does not exhibit any transitions up to 30 GPa,[13,20] while for experiments performed with silicone oil, methanol-ethanol 4:1 mixture or without PTM, a considerable broadening of Bragg peaks was observed, attributed to the pressure induced amorphization (PIA) with the onset at 15 GPa[20]. In the same report, Raman spectra of arsenolite with (4:1) methanol-ethanol mixture as the PTM and without PTM, revealed splitting and broadening of several modes above 3-6 GPa. Sans *et al.* attribute these changes to strengthening of intermolecular interactions and exclude the occurrence of a phase transition. In a previous contribution based on Raman and infrared spectroscopy studies of arsenolite in CsI as the PTM, Grzechnik claimed that the crystal undergoes a phase transition to a tetragonal phase at 4 GPa,[21] although a recent study shows that deviations from the hydrostatic conditions in CsI become significant above ~3 GPa[22]. Senarmontite, a cubic antimony oxide isostructural to arsenolite, shows markedly different high-pressure behavior. Previous XRD experiments conducted in methanol-ethanol 4:1 PTM evidence no symmetry changes up to 18 GPa, while subtle anomalies in pressure dependence of Raman modes may indicate two second-order phase transitions at 3.5 GPa and 10 GPa[23]. However, a later study of senarmontite in Ne unveiled a first-order phase transition to a layered tetragonal ($P\bar{4}2_1c$) phase beginning at ~15 GPa, followed by a sluggish amorphization above 25 GPa.[14]

In contrast to other cage compounds, reports on phase behavior of urotropine are rather scarce. The fully ordered room-temperature cubic urotropine phase is stable also at low temperature

down to 15 K.[24,25] A previous high-pressure study of urotropine (experiments carried out without PTM) was based solely on pressure evolution of Raman spectra suggesting two phase transitions around 1.4 GPa and 12.5 GPa, without providing structural information.[26] Besides, our discovery of pressure-induced helium penetration into single crystals of arsenolite begs the question of whether helium can permeate the crystal of urotropine composed of similar globular molecules.[13] The suggestion of localized interactions between trapped He atoms and As atoms featuring active lone electron pairs in $As_4O_6 \cdot 2He$ provides additional stimulus to seek for similar host-guest complexes of urotropine engaging lone pairs of nitrogen atoms.[20] Considering the above, it is therefore the purpose of this communication to investigate thoroughly urotropine behavior at high pressure using different PTM by combining single-crystal X-ray diffraction structural analysis and infrared absorption spectroscopy. In addition, DFT calculations were carried out to provide accurate description of the molecular structure of urotropine as a function of pressure.

MATERIALS AND METHODS

X-ray diffraction

Urotropine was purchased from Sigma Aldrich and single crystals suitable for X-ray diffraction were obtained by sublimation at reduced pressure and freshly used for the investigations. Urotropine single crystals were loaded together with ruby spheres into diamond anvil cells (DACs). Diamond anvils with 600-μm culets and stainless-steel gaskets preindented to a thickness of 75 μm with 300-μm diameter holes were used. Diffraction data were collected with a MAR 165 CCD detector at the ID27 beamline (λ = 0.3738 Å) and with a Mar555 flat-panel detector at the ID15B beamline (λ = 0.4110 Å) of the European Synchrotron Radiation Facility (Grenoble, France). Pressure was determined by the ruby fluorescence shift method.[27,28] Detector distance was calibrated using CeO_2 and Si powder standards on ID27 and ID15B

beamlines, respectively, whereas other instrument model parameters were determined from single-crystal diffraction experiments on enstatite crystals enclosed in DACs. Two runs with He used as the PTM were carried out on both beamlines and one run with Ne used as the PTM only on ID15B. He is a PTM with the highest known freezing pressure (11.8 GPa), and even in the solid state maintains quasihydrostatic conditions particularly well up to 23 GPa, as derived by pressure gradient.[29] Ne solidifies at 4.8 GPa and shows the first signs of nonhydrostaticity around 15 GPa, and even above this pressure, gradients are very small (less than 0.5 GPa at an average pressure of 50 GPa).[29] DACs were rotated from −32 to +32º and diffraction images were collected every 1º with an exposure time of 10 s at ID27 and every 0.5º with an exposure time of 1 s at the ID15B beamline. Additionally, wide scans were taken at some pressures with DACs rotated in the same angular range. These data and single-crystal diffraction were processed and analyzed using Dioptas and CrysAlis^{PRO} software, respectively.[30,31] Urotropine crystal structures were refined using SHELXL invoked from within Olex2 suite and analyzed with PLATON program.[32–34] Hydrogen atoms were placed at calculated positions and were refined as riding atoms. CCDC 1982556-1982593 records contain the supplementary crystallographic data for this paper. These data can be obtained free of charge from the joint CCDC's and FIZ Karlsruhe's service to view and retrieve structures via https://www.ccdc.cam.ac.uk/structures/. The wide scans integrated with Dioptas were analysed using GSAS-II.[35]

Hirshfeld Atom Refinements (HARs) were carried out for the diffraction data collected on ID15B beamline with He used as PTM using the HARt module implemented in Olex2.[36–38] Def2-TZVP basis set and restricted Kohn-Sham Hamiltonian along with BLYP exchange-correlation functional were employed.[39,40] Clusters of charges around central molecules were not

generated. Hydrogen anisotropic displacement parameters were refined while extinction was not accounted for.

DFT computations

Periodic boundary density functional theory (DFT) computations of urotropine crystal structure and energy under high pressure were carried out using pob-TZVP atom-centered Gaussian-type basis set in CRYSTAL09.[41–43] Crystal structures of urotropine were optimized under set external hydrostatic pressure up to 20 GPa using the B3LYP exchange-correlation functional with the Civalleri's D* correction accounting for dispersion interactions.[44] XL grid was used for charge integration in real space and Γ centered Monkhorst-Pack grid with a shrinking factor of 8 was used for integration in reciprocal space. SCF was considered converged when energy difference between consecutive steps was smaller than 10^{-8} Ha and the Broyden method was applied to speed up SCF convergence.[45] Geometry optimizations were performed in internal redundant coordinates until RMS of gradients and displacements were smaller than 0.00003 a.u. and 0.00012 a.u., respectively, and the energy difference between following steps was smaller than 10^{-8} Ha. The TOLINTEG parameters were set to "7 7 7 7 16". The same parameters were applied for the calculation of IR-active modes' wavenumbers.

Infrared spectroscopy

Fourier transform infrared (FTIR) absorption measurements were carried out at the European Laboratory for Non-linear Spectroscopy LENS, using a Bruker-IFS 120HR spectrometer adapted for high-pressure studies.[46,47] Urotropine was purified by sublimation and ground to powder before the experiment. Membrane DACs equipped with 600 μm culet diamonds and stainless-steel gaskets preindented initially to 50 μm with a 300 μm diameter hole were applied. Dried and finely milled KBr was packed into the gasket hole forming a pellet and filling the sample

chamber. A thin layer of KBr was subsequently scooped out with a needle tip. Then, the sample was deposited on the top of KBr substrate, deformed plastically and encapsulated uniformly upon closing the DAC. Using this method, infrared spectra could be obtained with reasonable absorbance without saturation. As KBr is transparent throughout the entire IR region, it does not contribute to any interfering absorbance bands. The second DAC was prepared likewise, but a top of the sample slab was eventually excavated to a depth of several microns, leaving space between the two-layered sandwich pellet and the top diamond. This cavity was then cryogenically loaded with nitrogen, ensuring (quasi)hydrostatic compression over a wider pressure range. In both loadings, ruby spheres were placed in the DACs along with the sample to allow pressure determination with the ruby florescence scale.[27,28] The parameters (frequency, width and intensity) of the infrared absorption bands were determined using the Fityk program by fitting Voigt profiles after manual baseline subtraction.[48]

It should be emphasized that KBr undergoes a phase transition at 2.14 GPa associated with a volume collapse of about 10%.[22,49] While below the transformation, KBr can be considered quasihydrostatic, above this threshold, substantial nonhydrostatic stresses are generated, reaching 1 GPa at 6 GPa pressure. Contrarily, nitrogen is seemingly a much better PTM in respect to its hydrostaticity range. LeSar *et al.* noted that linewidths of ruby fluorescence peaks and the observed R-line splitting remained constant up to ~13 GPa.[50] More recently Klotz *et al.* revised this value by investigating the pressure gradients from measurements of several ruby spheres equally distributed across the DAC sample chamber, concluding that the gradients rapidly increase beyond 10 GPa, reaching 0.6–0.8 GPa at ~25 GPa.[29] This threshold is indeed much higher than the solidification pressure of nitrogen 2.4 GPa and shows that in terms of hydrostaticity nitrogen is comparable to neon until 10 GPa, although the gradient rises more

steeply in the case of N_2 above this pressure. Remarkably, Angel *at al.* found the onset of non-hydrostaticity marked by the broadening of the X-ray diffraction peaks corresponding to the shear stresses in nitrogen at much lower pressure of 3 GPa.[51] To sum up, on the basis of these literature data, we infer that there is a significant difference in hydrostatic behavior of KBr and N_2 as PTM.

RESULTS

Structural studies

Urotropine crystallizes in the cubic space group $I\bar{4}3m$ (no. 217) with two molecules exhibiting the symmetry of $\bar{4}3m$ (T_d) point group per unit cell, with the molecular center of gravity placed at the 2*a* Wyckoff position. Urotropine represents a peculiar case where the molecular symmetry is preserved in the site and the factor group (one molecule for primitive cell). The amine undergoes monotonic compression up to 19 GPa both in helium and in neon and the space group symmetry of the crystal is preserved up to the highest pressure (see Figure 1). The 3rd order Vinet equation of state (EoS) fitted to the (V, p) data points collected at ID15B with He used as PTM yields V_0 = 347.71(13) Å^3, B_0 = 8.53(16) GPa and B_0' = 9.29(12) (V_0 was not fixed in the fitting procedure and its uncertainty comes from the least square fit).[52,53] One of the reasons we carried out the experiments was to determine whether He permeates urotropine crystal structure in a similar manner to arsenolite. The fact that the unit cells determined for urotropine in Ne and He fall on the same EoS line indicates that He does not permeate it.

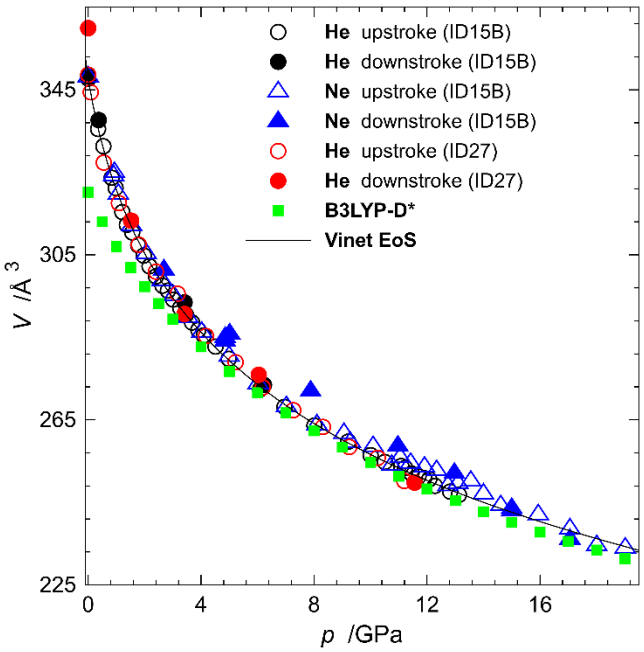

Figure 1. Urotropine unit cell volume plotted as a function of pressure for various experimental runs in He (circles; black and red correspond to data collected at the ID15B and ID27, respectively) and Ne (triangles) used as PTM. The experimental points are compared to DFT results denoted B3LYP-D* (small green filled squares). Markers are empty and filled for pressure increase and decrease, respectively. The black line corresponds to a 3rd order Vinet EoS fitted to the data collected at the ID15B beamline with He as PTM.

The dependence of experimentally determined C−N bond length on pressure exhibits a maximum around 3 GPa which is the result of two opposing effects: (1) C−N bond shortening and (2) quenching of libration with increasing pressure (see Figure 2 and Figure S1 for the dependence of C and N anisotropic displacement parameters (ADPs) on pressure). The second effect may seem counterintuitive, but it is not. Libration quenching with increasing pressure leads to apparent increase in bond lengths at low pressures. This is because at low pressures libration diminishes very significantly on pressure increase and its effect of apparent bond shortening falls relatively quickly leading to more realistic bond lengths *i.e.* longer bonds. At

higher pressures some residual libration persists and the apparent bond shortening does not change with pressure anymore (see the differences in uncorrected and corrected bond lengths in Figure 2). C−N bond lengths were corrected for libration using the approach proposed by Schomaker and Trueblood and the correction was performed using the PLATON program.[34,54] The idea of the correction lies in interpreting the ADPs of atoms constituting a molecule in terms of anisotropic translational and rotational oscillations of the molecule.[55] The effect of these angular oscillations is that the maxima of electron density appear to be closer to the center of rotations than they really are *i.e.* bonds seem to be shorter than they are. Cruickshank derived a formula to correct bond lengths for this effect and his formulation was later generalized by Schomaker and Trueblood.[56] Urotropine C−N bond lengths corrected for libration are in excellent agreement with the DFT computed bond lengths (see Figure 2). This, together with the fact that unit cell volumes of urotropine from DFT calculations are underestimated compared to experiment (see Figure 1), indicates two facts: (1) the contribution of phonons below 4 GPa significantly increases unit cell volume at RT compared to DFT-computed volume at 0 K and (2) dispersion interactions are in this particular case overestimated by the B3LYP-D* model.

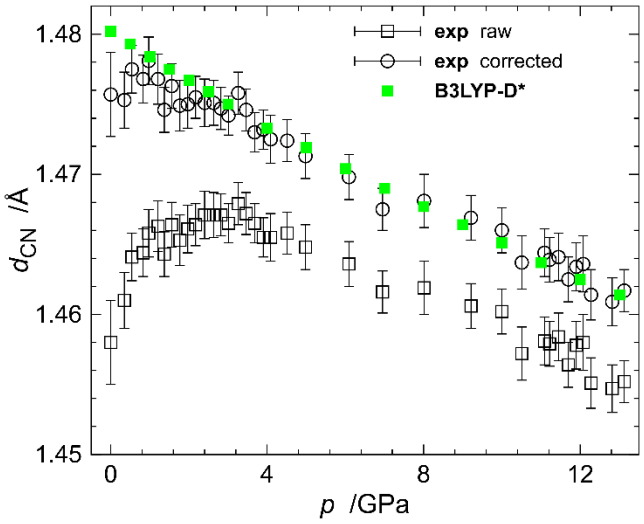

Figure 2. C−N bond lengths plotted as a function of pressure for the data collected with He used as PTM at the ID15B beamline. Squares and circles denote experimental bond lengths uncorrected and corrected for libration, respectively. Small green filled squares denote bond lengths obtained from periodic boundary DFT computations.

In the experiment carried out at the ID15B beamline with He used as PTM, we observed a phase transition in urotropine around 14 GPa, accompanied by a drop in unit cell volume of 3.30 $Å^3$ (1.30%). The crystal was completely transformed to a lower symmetry phase, which was accompanied by significant broadening of reflections (see Figure S2 for the raw images of wide scans before and after phase transition). We were able to index this phase using a primitive tetragonal *tP* unit cell with a = 5.7512(11) Å and c = 7.302(2) Å (at 14.08(12) GPa). This polymorph will be hereafter referred to as β while the cubic form will be referred to as α. The unit cell shrinks further with increasing pressure and three additional reflections located at 3.90º, 4.02º and 13.39º at 20.01(5) GPa began to appear (see Figure 3). They cannot be indexed using this unit cell. The formation of the β polymorph is attributed to uniaxial stress exerted on the studied crystal. Its initial size was ~50 x 40 x 30 μm^3 while the initial gasket thickness was 75 μm. Due to high He compressibility the gasket shrunk so much that the crystal bridged the diamonds and was subjected to substantial uniaxial stress which resulted in the phase transition. The crystal bridging was evidenced by interference fringes visible on the crystal face that touched the culet (see insets in Figure 3 for crystal photos in DAC under various pressures and Figure S3 for larger photos). The transition is reversible but there is a significant hysteresis. On pressure release we observed coexistence of two phases down to 9.04(11) GPa and the crystal transformed fully back into cubic phase at 6.23(7) GPa (see Figure 4 for unit cell parameters and Figure S4 for unit cell volume as a function of pressure plots). The analysis of the orientation

matrix and experimental setup geometry allowed us to conclude that the crystal was lying on the culet on the (111) face, indicating it was subjected to uniaxial compression along [111] crystallographic direction. Nonetheless, it did not undergo rhombohedral distortion but tetragonal. We did not observe such transition in the experiment on ID27 beamline because the crystal was not touched by the two diamonds then. Interestingly, wide scans carried out for a crystal pressurized in Ne reveal the coexistence of the tetragonal phase with the body center cubic one beginning from 12.74(8) GPa (see Figure S5). The intensities of reflections coming from the tetragonal phase are weak and increase with pressure indicating a slowly progressing phase transition. It can be concluded that the non-hydrostaticity of neon induces it too.

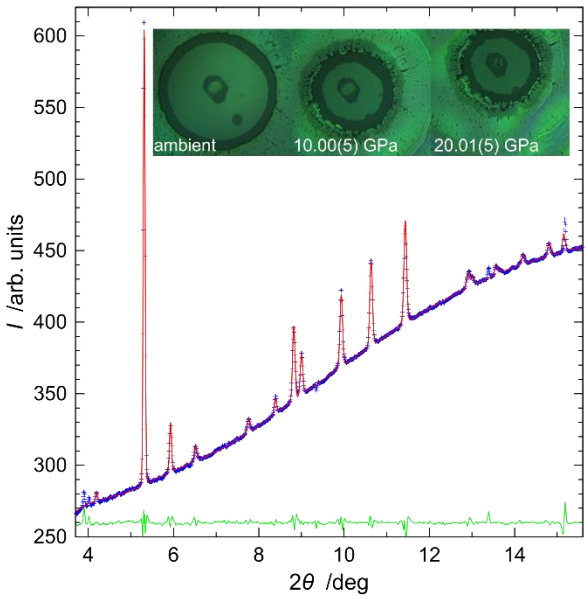

Figure 3. Integrated wide scan from the urotropine crystal bridged between two diamonds at 20.01(5) GPa and transformed into the β polymorph. Blue crosses and red line indicate experimental and calculated diffraction patterns, respectively. The green line is the difference between them plotted on the same scale and moved up to 250. Photographs of the studied crystal loaded in DAC at various pressures are presented in the inset.

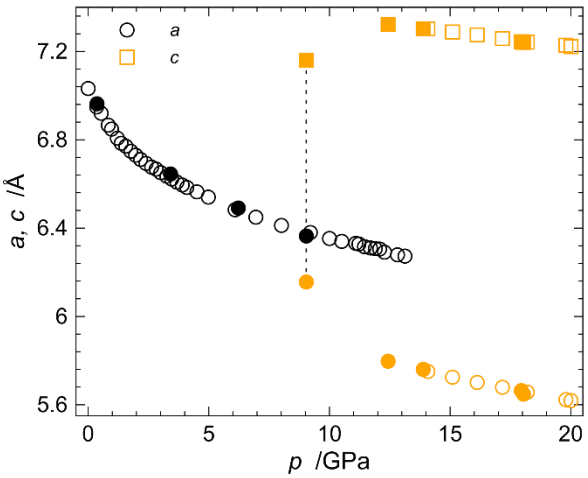

Figure 4. Unit cell parameters plotted as a function of pressure for the α and β polymorphs of urotropine. Black and orange symbols correspond to α and β unit cells, respectively, whereas open and closed symbols correspond to pressure increase and decrease, respectively.

Hirshfeld atom refinements

We attempted Hirshfeld atom refinement (HAR) for the α polymorph against the diffraction data collected at the ID15B beamline with He used as PTM to check whether it will be successful despite incomplete data sets resulting from the restrictions imposed on the experiment by the use of a DAC (completeness for the maximum attained 2θ value ranging from 58% to 78%) and whether it is possible to refine C−H bond lengths that would be in agreement with ones calculated by DFT.[36,37] HAR has recently been shown to give C−H bond lengths within one standard uncertainty of those coming from neutron diffraction measurements and with similar precision.[38] For our data sets, HAR was successful in most cases – only for two pressure points out of 36 did the refinement diverge. In the successful refinements, hydrogen atom ADPs were non positive definite in 7 cases and in three cases they were unphysical ("pancake" ADPs). For the other 26 cases, HAR refinement yielded realistic H atom ADPs. The C−N bond lengths were all within one standard uncertainty of the values obtained from conventional refinements. Carbon

and nitrogen ADPs did not differ much from the values from conventional spherical atom refinement either. The largest discrepancies for N ADPs were within 3 standard uncertainties and for C ADPs were generally smaller than 3 sigmas and for a few points as large as 6 sigmas. The C−H bond lengths from HAR oscillate around the C−H bond lengths coming from B3LYP-D* computations (see Figure 5). They are also within one standard uncertainty from the bond length of 1.10(2) Å determined from neutron diffraction experiment on urotropine single crystal carried out at ~0.25 GPa (*cf.* 1.13(3) Å at 0.35(5) GPa for our data).[57]

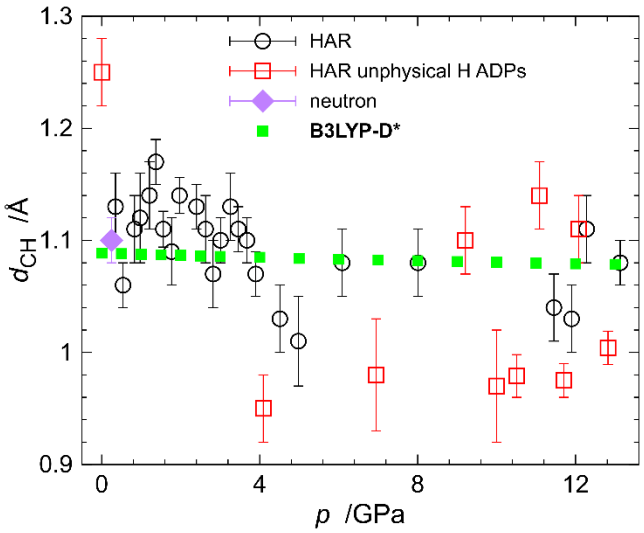

Figure 5. C−H bond lengths plotted as a function of pressure for the α polymorph of urotropine. Big black empty circles and small green filled circles denote bond lengths obtained from HAR and from periodic boundary DFT computations, respectively. Red empty squares indicate bond lengths from HAR in which H ADPs were non positive definite or "pancake-shaped". The purple diamond denotes bond length resulting from refinement against neutron diffraction data.

Infrared absorption spectroscopy

Urotropine FTIR absorption spectra plotted as a function of pressure are shown in Figure 6.

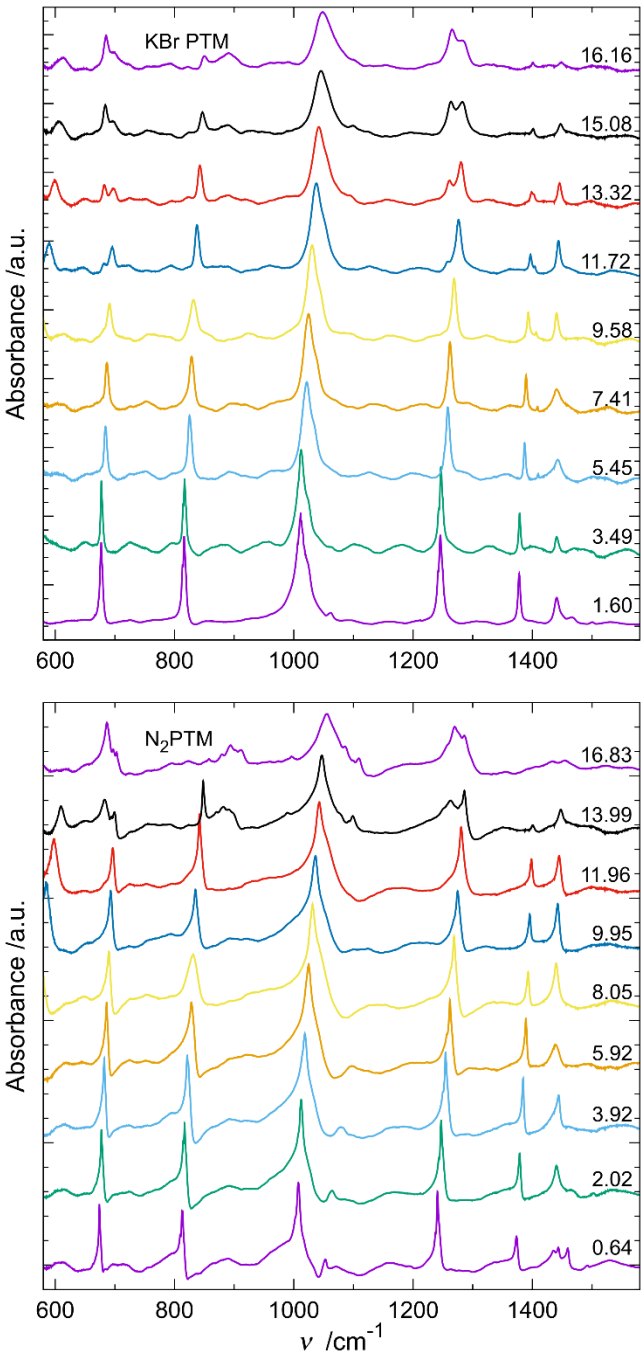

Figure 6. Pressure evolution of the infrared absorption spectrum of urotropine during the compression run in nitrogen (bottom) and KBr (top) PTM. Pressure values in GPa are reported above each spectrum.

Infrared bands are assigned according to literature data.[58] For the infrared analysis we selected the ν_{20} (1372.0 cm^{-1}), ν_{21} (1234.0 cm^{-1} for TO and 1238.0 cm^{-1} for LO component), and ν_{24} (674.2 cm^{-1} for both TO and LO components) bands because they are in-scale and isolated allowing a good fit in all experimental conditions. All the frequency values refer to ambient conditions. In nitrogen PTM, frequencies of both LO and TO components of the C−N bond ν_{21} stretching mode increase monotonically with pressure without major discontinuities (Figure 7, bottom panel). Near ~12 GPa a new band appears on the lower-frequency side of original ν_{21} modes and persists in decompression down to ~8 GPa, a point at which the frequencies of LO and TO modes revert to their prior values without hysteresis. Compression in KBr, however, shows apparent discontinuities in the slopes of ν_{21} LO and TO branches around ~4 GPa (Figure 7, top panel). Interestingly, the TO component at higher pressures behaves like the aforementioned new band appearing on compression in N_2 environment. We have therefore decided to analyze the line width of all the bands in the upstroke run. Plotting full width at half maximum (FWHM) as a function of pressure demonstrates that the width of ν_{21} LO component in the KBr PTM experiment is initially roughly constant, but triples abruptly between 9.6 and 10.0 GPa, coinciding with the appearance of the new component in nitrogen above this pressure (Figure S6). It can be therefore assumed that the ν_{21} LO component in KBr is the convolution of the LO-TO doublet observed in nitrogen, while the lower frequency component is a new band, which appears at lower pressure in the PTM with lower maximum limits of the hydrostatic behavior (KBr).

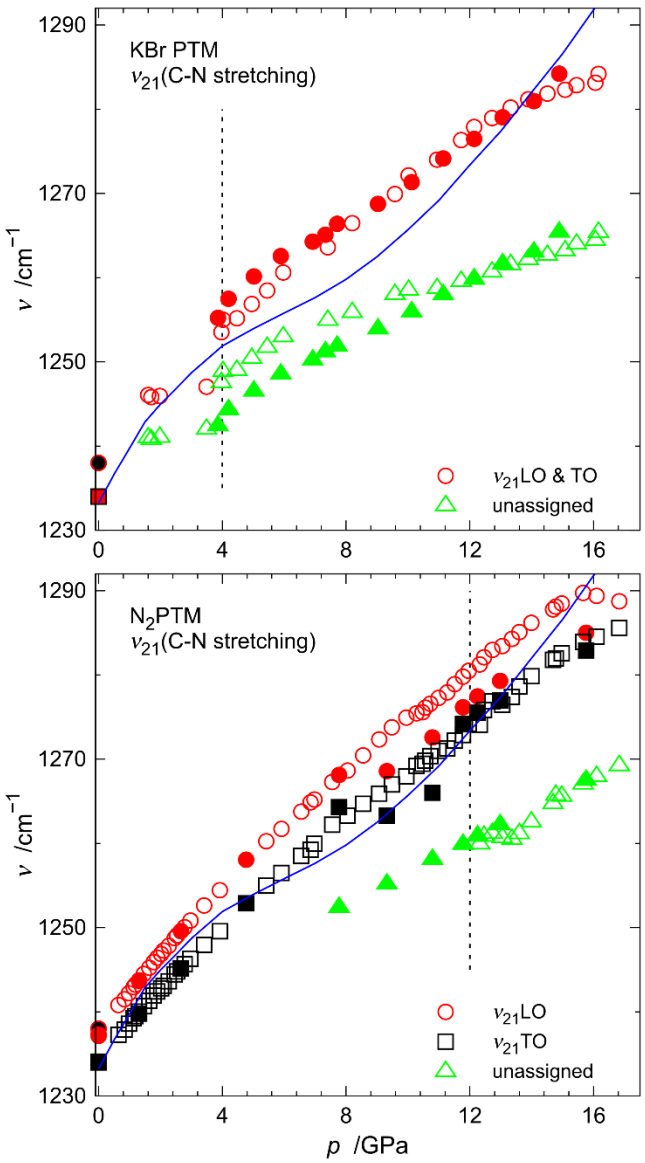

Figure 7. A variation of LO (red circles) and TO (black squares) components of ν_{21} C–N stretching mode plotted as a function of pressure in KBr (top) and N_2 (bottom) used as PTM. An additional unassigned band (green triangles) appears in compression in N_2 at about 12 GPa, persisting in decompression down to ~8 GPa. Full symbols refer to downstroke runs. Blue line corresponds to vibration frequencies calculated within the B3LYP-D* model and scaled by 0.975. Black circle with red border and red square with black border correspond to literature data at $p = 0$.[58]

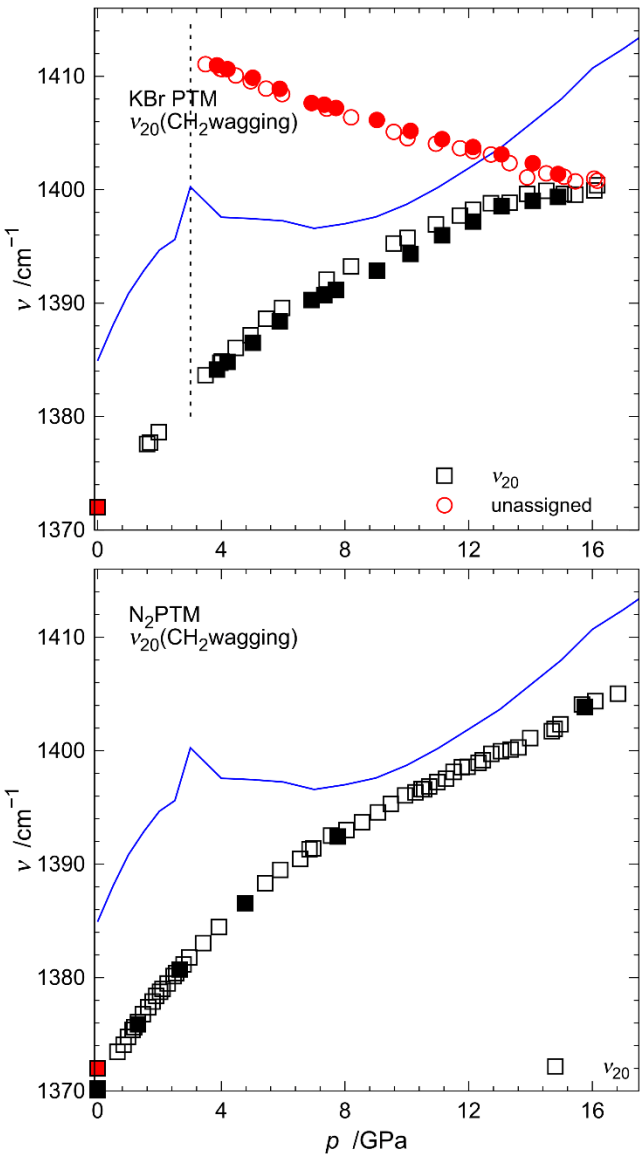

Figure 8. Pressure dependence of ν_{20} CH_2 wagging mode (black squares) plotted as a function of pressure in KBr (top) and N_2 (bottom) PTM. An unassigned soft mode (red circles) appears only in the compression in KBr PTM between 2.0 and 3.5 GPa. Filled symbols refer to downstroke runs. Blue line corresponds to vibration frequencies calculated within the B3LYP-D* model and scaled by 0.975. Red square with black border corresponds to literature data at $p = 0$.[58]

The CH_2 wagging mode ν_{20} follows the same regular continuous pressure dependence in both N_2 and KBr PTM, with a small hysteresis observable only in the sample compressed in KBr.

Surprisingly, between 2.0 and 3.5 GPa a soft mode appears in KBr, which is absent in the sample compressed quasihydrostatically in nitrogen (Figure 8). The appearance of the new band is associated with the intensity inversion of the bands in the C−H stretching mode regions (Figure S7). It is plausible that the new band might possibly be a Raman mode activated by stress.[58] Considering that the symmetry of the system does not change from molecule to crystal factor group, thus maintaining the same selection rules of the isolated molecule, lowering of the site symmetry by stress could activate the soft mode mentioned above.

For the ν_{24} C−N−C deformation mode, an analogous behavior is observed for both experiments. For the sample in N_2 PTM, a new band at a lower frequency side appears at ~12 GPa and persists on decompression down to 7-8 GPa. The frequency of the ν_{24} mode remains lower in decompression down to the pressure at which the new band disappears. In case of the sample compressed in KBr, the new band appears at 9-10 GPa and remains down to 4 GPa, *i.e.* the minimum pressure reached on the decompression run (Figure 9). Since at the atmospheric pressure the ν_{24} band is a superposition of TO and LO modes appearing at the same frequency,[58] it can be supposed that the observation of the new band is actually related to the pressure-induced component splitting.

Wavenumbers of urotropine IR-active vibrational bands were calculated using the B3LYP-D* model and are presented in Figure S8 and a selection of them in Figures 7-9. It is noteworthy that the calculated wavenumbers exhibit discontinuities for all IR-active modes around 4 GPa.

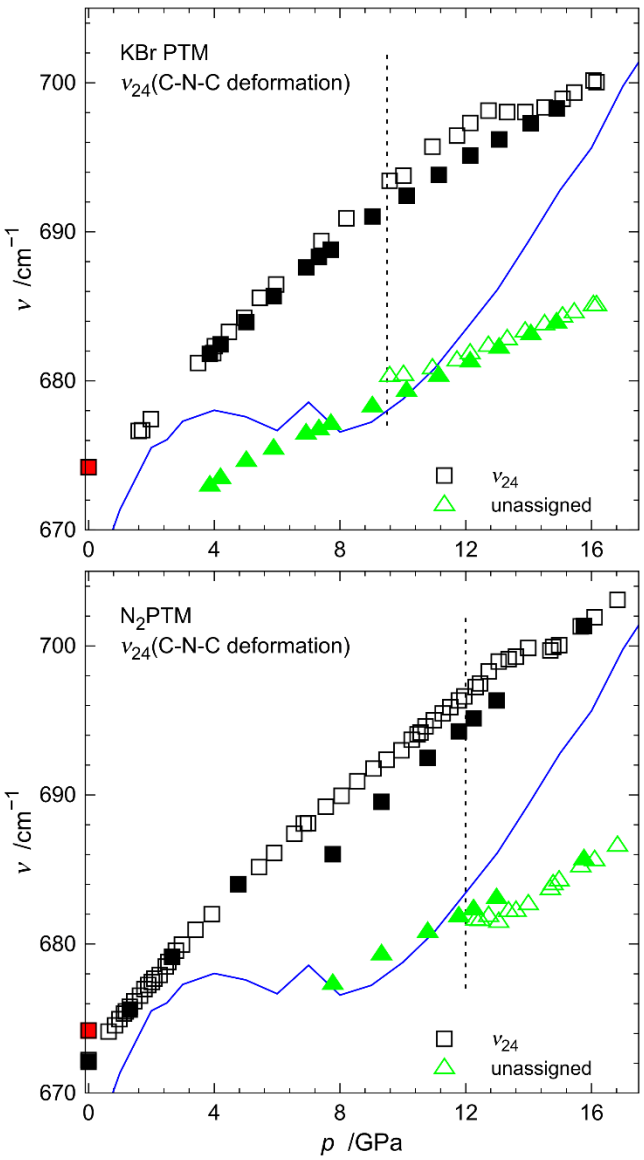

Figure 9. Pressure dependence of ν_{24} C−N−C wagging mode (black squares) plotted as a function of pressure together with a new unassigned band that appears on compression (green triangles) in KBr (top) and N_2 (bottom) PTM. Filled symbols refer to downstroke runs. Blue line corresponds to vibration frequencies calculated within the B3LYP-D* model and scaled by 0.975. Red square with black border corresponds to literature data at $p = 0$.[58]

DISCUSSION AND CONCLUSIONS

Investigation of the effects of pressure on crystalline urotropine revealed two structural changes in the pressure behavior. The first one is more subtle and not attributed to any apparent discontinuity in the unit-cell volume. It manifests in the damping of atomic thermal motions evidenced by decrease in the ADP magnitudes of C and N atoms with pressure (Figure S1) and suppressed C−N bond libration (Figure 2), both completed at ~4 GPa, as well as discontinuities in calculated wavenumbers of IR-active modes at this pressure. Remarkably, the static zero-kelvin DFT calculations understate unit-cell volume up to this critical pressure value. Therefore, it can suggest that the system plausibly undergoes an isostructural second-order transformation of disorder-order type, related to the reduced amplitude of atomic motions or a transition associated with hindering collective molecular rotations about their symmetry elements. Surprisingly, while all these structural features were observed in a diffraction experiment performed under strictly hydrostatic conditions and in calculations where hydrostatic stress was exerted on urotropine, no anomaly was observed in this pressure range in infrared spectra of the urotropine sample in nitrogen PTM. However, in non-hydrostatic PTM (KBr) some abrupt changes become evident around 4 GPa, as discontinuities in the slopes of the C−N bond ν_{21} stretching mode LO and TO components and appearance of the new soft mode near ν_{20} CH_2 wagging band. It is pertinent to note here that the literature Raman data collected for the sample without PTM suggest the first transition around 1.4 GPa.[26]

The second recorded structural change is an evident first-order phase transition associated with a symmetry lowering from cubic to tetragonal, an abrupt change of lattice parameters and a drop of the unit cell volume beginning at ~12.7 GPa in the experiments carried out at ID15B conducted in Ne and ~14 GPa in He. In the case of the sample in He, the transition onset

coincides with the pressure at which the sample begins to bridge the anvils. Meanwhile, in the XRD experiments performed at ID27, no evidence of phase transition could be detected up to 19 GPa. FTIR experiments in N_2 PTM revealed the appearance of new bands at ~12 GPa: (1) on the lower-frequency side of original C−N bond ν_{21} stretching modes and (2) on the lower-frequency side of the ν_{21} C−N−C deformation mode. Interestingly, the new band on the lower-frequency side of the ν_{21} mode appears also for the sample compressed in KBr PTM, but with an onset at lower pressure (9-10 GPa). Noteworthy, this pressure values agree well with the literature limit of the second phase transition of 12.5 GPa postulated in the Raman study.[26] The new bands can be related to the symmetry lowering associated with the transition which causes the activation of new Davydov components. All methods indicate a sluggish character and a considerable hysteresis of this phase change.

Deviatoric stress is known to influence strongly behavior of materials at high pressure, from perturbed determination of lattice parameters to the diverse stability fields of phases. Generally avoided by a careful choice of pressure transmitting medium, sometimes it can provide useful insights and perspectives in solid state chemistry and physics.[59] Earlier studies of analogous cage-like molecules crystallizing in cubic structures at ambient conditions, like diamantane [19] and arsenolite[21], revealed phase transformations occurring only at non-hydrostatic conditions and proceeding with desymmetrization of the crystal lattice. In this respect, urotropine follows the same path, transforming to the tetragonal structure only when subjected to deviatoric stress. Hence, this kind of behavior manifesting only under anisotropic compression may be more common in highly symmetric cage-like molecular systems, which otherwise seem to be remarkably stable up to surprisingly high pressures.

ASSOCIATED CONTENT

Supporting Information. The following files are available free of charge.

plots of ADPs, urotropine unit cell volume and bands FWHM as a function of pressure, urotropine crystal microphotographs, integrated diffraction patterns in Ne, evolution of urotropine IR spectra and comparison of experimental and DFT computed bands' wavenumbers (PDF)

results of conventional structural refinements (within independent atom model) (CIF)

results of HAR (CIF)

AUTHOR INFORMATION

Corresponding Authors

*piogun@ch.pw.edu.pl (P.A.G.) dziubek@lens.unifi.it (K.F.D.)

Present Addresses

†I.E.C. Center for X-ray Analytics, Swiss Federal Laboratories for Materials Science and Technology, Überlandstrasse 129, 8600 Dübendorf, Switzerland.

Author Contributions

All authors have given approval to the final version of the manuscript.

ACKNOWLEDGMENT

Calculations have been carried out by using resources provided by the Wroclaw Centre for Networking and Supercomputing (http://wcss.pl), grant no. 260. We acknowledge the European Synchrotron Radiation Facility (ESRF) for provision of synchrotron radiation facilities. M. Hanfland and J. Jacobs are acknowledged for gas loading of the DACs for the ID15B beamtime.

The Polish contribution to the ESRF budget was financed by the Polish Ministry of Science and High Education – decision number: DIR/WK/2016/19.

REFERENCES

(1) Mak, T. C. W.; Mok, F.-C. Inorganic Cages Related to Cubane and Adamantane. *J. Cryst. Mol. Struct.* **1978**, *8* (4), 183–191. https://doi.org/10.1007/BF01297662.

(2) Pertlik, F. Structure Refinement of Cubic As_2O_3 (Arsenolite) with Single-Crystal Data. *Czech. J. Phys.* **1978**, *28* (2), 170–176.

(3) Butlerow, A. Ueber Einige Derivate Des Jodmethylens. *Ann. Chem. Pharm.* **1859**, *111* (2), 242–252. https://doi.org/10.1002/jlac.18591110219.

(4) Butlerow, A. Ueber Ein Neues Methylenderivat. *Ann. Chem. Pharm.* **1860**, *115* (3), 322–327. https://doi.org/10.1002/jlac.18601150325.

(5) Roose, P.; Eller, K.; Henkes, E.; Rossbacher, R.; Höke, H. Amines, Aliphatic. In *Ullmann's Encyclopedia of Industrial Chemistry*; Wiley-VCH Verlag GmbH & Co. KGaA, 2015; pp 1–55. https://doi.org/10.1002/14356007.a02_001.pub2.

(6) Briani, G.; Fray, N.; Cottin, H.; Benilan, Y.; Gazeau, M.-C.; Perrier, S. HMT Production and Sublimation during Thermal Process of Cometary Organic Analogs. Implications for Its Detection with the ROSETTA Instruments. *Icarus* **2013**, *226* (1), 541–551. https://doi.org/10.1016/j.icarus.2013.05.038.

(7) Groom, C. R.; Bruno, I. J.; Lightfoot, M. P.; Ward, S. C. The Cambridge Structural Database. *Acta Crystallogr. Sect. B* **2016**, *72* (2), 171–179. https://doi.org/10.1107/S2052520616003954.

(8) Kirillov, A. M. Hexamethylenetetramine: An Old New Building Block for Design of Coordination Polymers. *Coord. Chem. Rev.* **2011**, *255* (15), 1603–1622. https://doi.org/10.1016/j.ccr.2011.01.023.

(9) Dickinson, R. G.; Raymond, A. L. The Crystal Structure of Hexamethylene-Tetramine. *J. Am. Chem. Soc.* **1923**, *45* (1), 22–29. https://doi.org/10.1021/ja01654a003.

(10) Gonell, H. W.; Mark, H. Röntgenographische Bestimmung Der Strukturformel Des Hexamethylentetramins. *Z. Phys. Chem.* **1923**, *107U* (1), 181–218. https://doi.org/10.1515/zpch-1923-10715.

(11) Brock, C. P.; Dunitz, J. D. Towards a Grammar of Crystal Packing. *Chem. Mater.* **1994**, *6* (8), 1118–1127. https://doi.org/10.1021/cm00044a010.

(12) Karle, I. L.; Karle, J. The Crystal and Molecular Structure of Congressane, $C_{14}H_{20}$, by X-Ray Diffraction. *J. Am. Chem. Soc.* **1965**, *87* (4), 918–920. https://doi.org/10.1021/ja01082a043.

(13) Guńka, P. A.; Dziubek, K. F.; Gładysiak, A.; Dranka, M.; Piechota, J.; Hanfland, M.; Katrusiak, A.; Zachara, J. Compressed Arsenolite As_4O_6 and Its Helium Clathrate $As_4O_6 \cdot 2He$. *Cryst. Growth Des.* **2015**, *15* (8), 3740–3745. https://doi.org/10.1021/acs.cgd.5b00390.

(14) Zhao, Z.; Zeng, Q.; Zhang, H.; Wang, S.; Hirai, S.; Zeng, Z.; Mao, W. L. Structural Transition and Amorphization in Compressed α-Sb_2O_3. *Phys. Rev. B* **2015**, *91* (18), 184112. https://doi.org/10.1103/PhysRevB.91.184112.

(15) Vijayakumar, V.; Garg, A. B.; Godwal, B. K.; Sikka, S. K. High-Pressure Phase Transitions in Adamantane. *Chem. Phys. Lett.* **2000**, *330* (3), 275–280. https://doi.org/10.1016/S0009-2614(00)01074-5.

(16) Yildirim, T.; Gehring, P. M.; Neumann, D. A.; Eaton, P. E.; Emrick, T. Unusual Structure, Phase Transition, and Dynamics of Solid Cubane. *Phys. Rev. Lett.* **1997**, *78* (26), 4938–4941. https://doi.org/10.1103/PhysRevLett.78.4938.

(17) Huang, H.-T.; Zhu, L.; Ward, M. D.; Chaloux, B. L.; Hrubiak, R.; Epshteyn, A.; Badding, J. V.; Strobel, T. A. Surprising Stability of Cubane under Extreme Pressure. *J. Phys. Chem. Lett.* **2018**, *9* (8), 2031–2037. https://doi.org/10.1021/acs.jpclett.8b00395.

(18) Bertz, S. H.; Kourouklis, G. A.; Jayaraman, A.; Lannoye, G.; Cook, J. M. High-Pressure Raman Studies of Triquinacene and Dodecahedrane. *Can. J. Chem.* **1993**, *71* (3), 352–357. https://doi.org/10.1139/v93-052.

(19) Yang, F.; Lin, Y.; Dahl, J. E. P.; Carlson, R. M. K.; Mao, W. L. Deviatoric Stress-Induced Phase Transitions in Diamantane. *J. Chem. Phys.* **2014**, *141* (15), 154305. https://doi.org/10.1063/1.4897252.

(20) Sans, J. A.; Manjón, F. J.; Popescu, C.; Cuenca-Gotor, V. P.; Gomis, O.; Muñoz, A.; Rodríguez-Hernández, P.; Contreras-García, J.; Pellicer-Porres, J.; Pereira, A. L. J.; Santamaría-Pérez, D.; Segura, A. Ordered Helium Trapping and Bonding in Compressed Arsenolite: Synthesis of $As_4O_6 \cdot 2He$. *Phys. Rev. B* **2016**, *93* (5), 054102. https://doi.org/10.1103/PhysRevB.93.054102.

(21) Grzechnik, A. Compressibility and Vibrational Modes in Solid As_4O_6. *J. Solid State Chem.* **1999**, *144* (2), 416–422. https://doi.org/doi: 10.1006/jssc.1999.8189.

(22) Celeste, A.; Borondics, F.; Capitani, F. Hydrostaticity of Pressure-Transmitting Media for High Pressure Infrared Spectroscopy. *High Pressure Res.* **2019**, *39* (4), 608–618. https://doi.org/10.1080/08957959.2019.1666844.

(23) Pereira, A. L. J.; Gracia, L.; Santamaría-Pérez, D.; Vilaplana, R.; Manjón, F. J.; Errandonea, D.; Nalin, M.; Beltrán, A. Structural and Vibrational Study of Cubic Sb_2O_3 under High Pressure. *Phys. Rev. B* **2012**, *85* (17), 174108.

(24) Becka, L. N.; Cruickshank, D. W. J.; Cox, E. G. The Crystal Structure of Hexam Ethylenetetramine I. X -Ray Studies at 298, 100 and 34 °K. *Proc. R. Soc. London, Ser. A* **1963**, *273* (1355), 435–454. https://doi.org/10.1098/rspa.1963.0101.

(25) Kampermann, S. P.; Sabine, T. M.; Craven, B. M.; McMullan, R. K. Hexamethylenetetramine: Extinction and Thermal Vibrations from Neutron Diffraction at Six Temperatures. *Acta Cryst A* **1995**, *51* (4), 489–497. https://doi.org/10.1107/S0108767394013711.

(26) Rao, R.; Sakuntala, T.; Deb, S. K.; Roy, A. P.; Vijayakumar, V.; Godwal, B. K.; Sikka, S. K. High-Pressure Raman Scattering Studies on Hexamethylenetetramine. *Chemical Physics Letters* **1999**, *313* (5–6), 749–754. https://doi.org/10.1016/S0009-2614(99)01069-6.

(27) Mao, H. K.; Xu, J.; Bell, P. M. Calibration of the Ruby Pressure Gauge to 800 Kbar under Quasi-Hydrostatic Conditions. *J. Geophys. Res.: Solid Earth* **1986**, *91* (B5), 4673–4676. https://doi.org/10.1029/JB091iB05p04673.

(28) Syassen, K. Ruby under Pressure. *High Pressure Res.* **2008**, *28* (2), 75–126. https://doi.org/10.1080/08957950802235640.

(29) Klotz, S.; Chervin, J.-C.; Munsch, P.; Marchand, G. L. Hydrostatic Limits of 11 Pressure Transmitting Media. *J. Phys. D* **2009**, *42* (7), 075413. https://doi.org/10.1088/0022-3727/42/7/075413.

(30) Prescher, C.; Prakapenka, V. B. DIOPTAS: A Program for Reduction of Two-Dimensional X-Ray Diffraction Data and Data Exploration. *High Pressure Res.* **2015**, *35* (3), 223–230. https://doi.org/10.1080/08957959.2015.1059835.

(31) *CrysAlisPro Software System Ver. 171.40.71a*; Rigaku OD: Oxford, UK, 2019.

(32) Sheldrick, G. M. Crystal Structure Refinement with SHELXL. *Acta Crystallogr. Sect. C* **2015**, *71* (1), 3–8. https://doi.org/10.1107/S2053229614024218.

(33) Dolomanov, O. V.; Bourhis, L. J.; Gildea, R. J.; Howard, J. A. K.; Puschmann, H. OLEX2: A Complete Structure Solution, Refinement and Analysis Program. *J. Appl. Crystallogr.* **2009**, *42* (2), 339–341. https://doi.org/10.1107/S0021889808042726.

(34) Spek, A. L. Single-Crystal Structure Validation with the Program It PLATON. *J. Appl. Crystallogr.* **2003**, *36* (1), 7–13. https://doi.org/10.1107/S0021889802022112.

(35) Toby, B. H.; Von Dreele, R. B. GSAS-II: The Genesis of a Modern Open-Source All Purpose Crystallography Software Package. *J. Appl. Crystallogr.* **2013**, *46* (2), 544–549.

(36) Jayatilaka, D.; Dittrich, B. X-Ray Structure Refinement Using Aspherical Atomic Density Functions Obtained from Quantum-Mechanical Calculations. *Acta Crystallogr. Sect. A* **2008**, *64* (3), 383–393. https://doi.org/10.1107/S0108767308005709.

(37) Capelli, S. C.; Bürgi, H.-B.; Dittrich, B.; Grabowsky, S.; Jayatilaka, D. Hirshfeld Atom Refinement. *IUCrJ* **2014**, *1* (5), 361–379. https://doi.org/10.1107/S2052252514014845.

(38) Woińska, M.; Grabowsky, S.; Dominiak, P. M.; Woźniak, K.; Jayatilaka, D. Hydrogen Atoms Can Be Located Accurately and Precisely by X-Ray Crystallography. *Science Advances* **2016**, *2* (5), e1600192. https://doi.org/10.1126/sciadv.1600192.

(39) Weigend, F.; Ahlrichs, R. Balanced Basis Sets of Split Valence, Triple Zeta Valence and Quadruple Zeta Valence Quality for H to Rn: Design and Assessment of Accuracy. *Phys. Chem. Chem. Phys.* **2005**, *7* (18), 3297–3305. https://doi.org/10.1039/B508541A.

(40) Kohn, W.; Sham, L. J. Self-Consistent Equations Including Exchange and Correlation Effects. *Phys. Rev.* **1965**, *140* (4A), A1133–A1138.

(41) Dovesi, R.; Orlando, R.; Civalleri, B.; Roetti, C.; Saunders, V. R.; Zicovich-Wilson, C. M. CRYSTAL: A Computational Tool for the *Ab Initio* Study of the Electronic Properties of Crystals. *Z. Kristallogr.* **2005**, *220* (5–6), 571–573. https://doi.org/10.1524/zkri.220.5.571.65065.

(42) Dovesi, R.; Saunders, V. R.; Roetti, C.; Orlando, R.; Zicovich-Wilson, C. M.; Pascale, B.; Civalleri, B.; Doll, K.; Harrison, N. M.; Bush, I. J.; D'Arco, P.; Llunell, M. *CRYSTAL09*; University of Torino, Torino, 2009.

(43) Peintinger, M. F.; Oliveira, D. V.; Bredow, T. Consistent Gaussian Basis Sets of Triple-Zeta Valence with Polarization Quality for Solid-State Calculations. *J. Comput. Chem.* **2013**, *34* (6), 451–459. https://doi.org/10.1002/jcc.23153.

(44) Civalleri, B.; Zicovich-Wilson, C. M.; Valenzano, L.; Ugliengo, P. B3LYP Augmented with an Empirical Dispersion Term (B3LYP-D*) as Applied to Molecular Crystals. *CrystEngComm* **2008**, *10* (4), 405–410. https://doi.org/10.1039/B715018K.

(45) Johnson, D. D. Modified Broyden's Method for Accelerating Convergence in Self-Consistent Calculations. *Phys. Rev. B* **1988**, *38* (18), 12807–12813.

(46) Bini, R.; Ballerini, R.; Pratesi, G.; Jodl, H. J. Experimental Setup for Fourier Transform Infrared Spectroscopy Studies in Condensed Matter at High Pressure and Low Temperatures. *Rev. Sci. Instrum.* **1997**, *68* (8), 3154–3160. https://doi.org/10.1063/1.1148261.

(47) Gorelli, F. A.; Ulivi, L.; Santoro, M.; Bini, R. The ε Phase of Solid Oxygen: Evidence of an O_4 Molecule Lattice. *Phys. Rev. Lett.* **1999**, *83* (20), 4093–4096. https://doi.org/10.1103/PhysRevLett.83.4093.

(48) Wojdyr, M. Fityk: A General-Purpose Peak Fitting Program. *J. Appl. Crystallogr.* **2010**, *43* (5), 1126–1128. https://doi.org/10.1107/S0021889810030499.

(49) Zhao, J.; Ross, N. L. Non-Hydrostatic Behavior of KBr as a Pressure Medium in Diamond Anvil Cells up to 5.63 GPa. *J. Phys.: Condens. Matter* **2015**, *27* (18), 185402. https://doi.org/10.1088/0953-8984/27/18/185402.

(50) LeSar, R.; Ekberg, S. A.; Jones, L. H.; Mills, R. L.; Schwalbe, L. A.; Schiferl, D. Raman Spectroscopy of Solid Nitrogen up to 374 Kbar. *Solid State Commun.* **1979**, *32* (2), 131–134. https://doi.org/10.1016/0038-1098(79)91073-1.

(51) Angel, R. J.; Bujak, M.; Zhao, J.; Gatta, G. D.; Jacobsen, S. D. Effective Hydrostatic Limits of Pressure Media for High-Pressure Crystallographic Studies. *J. Appl. Crystallogr.* **2007**, *40* (1), 26–32. https://doi.org/10.1107/S0021889806045523.

(52) Vinet, P.; Ferrante, J.; Smith, J. R.; Rose, J. H. A Universal Equation of State for Solids. *J. Phys. C: Solid State Phys.* **1986**, *19* (20), L467–L473. https://doi.org/10.1088/0022-3719/19/20/001.

(53) Vinet, P.; Ferrante, J.; Rose, J. H.; Smith, J. R. Compressibility of Solids. *J. Geophys. Res.: Solid Earth* **1987**, *92* (B9), 9319–9325. https://doi.org/10.1029/JB092iB09p09319.

(54) Schomaker, V.; Trueblood, K. N. On the Rigid-Body Motion of Molecules in Crystals. *Acta Crystallogr. Sect. B* **1968**, *24* (1), 63–76. https://doi.org/10.1107/S0567740868001718.

(55) Cruickshank, D. W. J. The Analysis of the Anisotropic Thermal Motion of Molecules in Crystals. *Acta Crystallogr.* **1956**, *9* (9), 754–756. https://doi.org/10.1107/S0365110X56002047.

(56) Cruickshank, D. W. J. Errors in Bond Lengths Due to Rotational Oscillations of Molecules. *Acta Crystallogr.* **1956**, *9* (9), 757–758. https://doi.org/10.1107/S0365110X56002059.

(57) Binns, J.; Kamenev, K. V.; McIntyre, G. J.; Moggach, S. A.; Parsons, S. Use of a Miniature Diamond-Anvil Cell in High-Pressure Single-Crystal Neutron Laue Diffraction. *IUCrJ* **2016**, *3* (3), 168–179. https://doi.org/10.1107/S2052252516000725.

(58) Bertie, J. E.; Solinas, M. Infrared and Raman Spectra and the Vibrational Assignment of Hexamethylenetetramine-h12 and -d12. *J. Chem. Phys.* **1974**, *61* (5), 1666–1677. https://doi.org/10.1063/1.1682160.

(59) Bassett, W. A. Deviatoric Stress: A Nuisance or a Gold Mine? *J. Phys.: Condens. Matter* **2006**, *18* (25), S921–S931. https://doi.org/10.1088/0953-8984/18/25/S01.

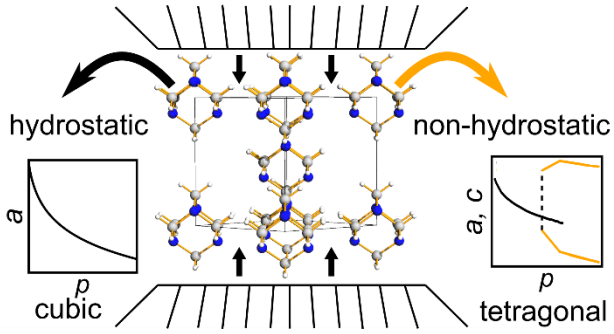
hydrostatic
non-hydrostatic
a
p
cubic
a, c
p
tetragonal